Planar Photonic Crystals Biosensor Applications of TiO_2

U. Erdiven[a], M. Karaaslan[b,*], E. Unal[b] and F. Karadağ[a]

[a]Department of Physics, Çukurova University, Adana, 01140, Turkey

[b]Department of Electric and Electronic Engineering, University of Mustafa Kemal, Hatay, 31140, Turkey

(Received November 29, 2011; in final form June 11, 2012)

We examine quality factor and sensitivity change depending on the resonant wavelength changing refractive index of surrounding liquid for TiO_2 photonic crystal slab structure. Photonic crystal slab structure is used widely for biological materials such as proteins, antigens, DNA, cells, virus particles and bacteria. Mentioned photonic crystal slabs are usable with large-area biosensor designs. They permit direct access to externally incident optical beams in a microfluidic device. Model calculations are based on two-dimensional periodic crystal structure. Photonic crystal slab consists of a square lattice of air holes in a finite-thickness dielectric slab. The time domain simulations were implemented by software MIT Electromagnetic Equation Propagation.

PACS: 78.67.Pt, 42.70.Qs, 07.07.Df, 42.79.Pw

1. Introduction

The rapid development of analytical equipment for characterizing molecular interactions has been driven over the last two decades by the increasing demand for a better understanding of the specific interactions among biomolecules, which provide insights into fundamental biological processes and serve as the cornerstones of life science research, pharmaceutical discovery, medical diagnosis, food/water safety assurance, environmental monitoring and biomolecular detection (protein, DNA, small molecules, viruses, cells, bacteria) and homeland security [1–4].

Label-free biosensors accomplish with suit of a few fundamental physical capacity connect to detecting biomolecular interactions and biological analytes that can include capture molecules, peptides, proteins, bacteria, or cells [5–8]. Photonic crystal (PC) label-free sensors are based on a periodic pattern or structure of dielectric material in two or three dimensions optimized to provide an extremely narrow resonant mode whose wavelength is particularly sensitive to modulations induced by the deposition of biochemical material on its surface. In practice, the sensor surface is illuminated with white light and the reflected light from different locations is collected. By analyzing the changes in the wavelength of the reflected light, biochemical binding events occurring on the surface can be detected and quantified. In general, label-free biosensing with optics relies on detecting changes in a local parameter such as absorption, refractive index (RI), or scattering [9, 10].

Extensively TiO_2 has been used for different applications such as DNA biosensor [11], enzyme immobilized platforms [12, 13], detection of *Pseudomonas aeruginosa* [14] and detection of toxic compounds [15], photonic crystal optical biosensor [16], atomic layer deposition [17] and electrochemical biosensor [18]. TiO_2 nanotubes have been used to immobilizing proteins and enzymes in biomaterial and biosensor applications because of high sensitivity at the near-infrared (750 nm) and near-ultraviolet (400 nm) wavelengths [19]. It has been demonstrated that the large surface area, good chemical stability and nontoxicity of the TiO_2 have been achieved with different nanocomposite and 3D macroporous structures [20, 21].

Beside this, TiO_2 is very important for many application areas such as, photocatalysts, sensors and solar cells. Since, TiO_2 have broad photonic bandwidth and optical absorption level is ten times less than that of the silicon at optical communication wavelength (1.5 μm) [22], it can restrict more easily to the guided resonance modes. Hence, incident wave couples easily with photonic crystals in microfluid for any biosensor.

Because of the high refractive index of TiO_2 photonic crystals, TiO_2 is transparent for broad bandwidth. Therefore, the fabrication and design of this type of PC with TiO_2 is very attractive for visible light wavelength. These properties are the basis of these structures as photocatalyst and sensor [22]. Although they have less sensitivity than some other sensors, we choose TiO_2 at PCs, since TiO_2 based PCs can be used for protein and analyte biosensing.

Comparing with traditional sensing techniques, it can be seen that nanoscale biosensors have advantages. Photonic crystal slab (PCS) devices are an important class of nanoscale biosensors [23]. A PCS is a one- or two-dimensional periodically patterned dielectric slab [24, 25]. In-plane guided modes confinement of light can be done by the higher refractive index (RI) dielectric material or can be guided resonance modes in the slab,

* corresponding author; e-mail: mkaraaslan@mersin.edu.tr

where coupling to externally incident optical beams is allowed [22]. The sensing by using guided resonance modes is very appealing.

PCs are now well acknowledged for their capability to control and manipulate the propagation of electromagnetic waves in confined space [26]. The work of Yablonovitch [27] and John [28] on such structures, often called photonic crystals, displays a range of frequency where propagation is completely forbidden. This is called the photonic band gap (PBG) and is analogous to the electronic band gap that is found in semiconductors. A photonic crystal structure may be designed to exhibit extraordinarily high reflection efficiency at particular wavelengths, at which optical standing waves develop and resonate within the photonic crystal structure. Such optical resonances are known to occur at the wavelengths adjacent to the photonic band gap, sometimes referred to as the photonic band edge. The spectral width and wavelength of the resonance phenomena describes the important externally measurable parameters of a device. Resonance width refers to the full width at half maximum, in wavelength measure, of a resonance feature plotted as transmittance versus wavelength.

In the past decade, several groups have studied the applications of TiO_2 PC structures for RI sensing [5, 20]. In this work, we emphasize the theoretical properties of RI sensing in PCS devices to enhancement of recent studies of TiO_2 photonic crystal-based sensor devices. We estimate properties for guided resonance modes associated with these devices and determine that the type of guided resonance mode supported by the PCS can result in notably different sensing characteristics. This difference is especially significant in symmetric PCS structures, where the slab is suspended in water.

2. Computational methods

There are many parameters to consider in evaluating the performance of biosensors, including sensitivity, resolution (or detection limit). These are different parameters, but they are also related to each other.

Sensor sensitivity is an important parameter in evaluating a sensor's performance. Sensitivity is defined as the ratio of the change in sensor output response to the change in the quantity to be measured. The expressions of the sensor's sensitivity depend on the detected change in the thickness or refractive index and the detection methods. For optical sensors, sensitivity is fundamentally determined by how efficiently the electromagnetic field interacts with biomolecules bound on the sensor surface or simply by the fraction of light in the solution or by the light intensity at the sensor surface [29]. So the bulk solvent refractive index sensitivity in the units of nm per refractive index unit (nm/RIU) reflects the fraction of light in the solution and enables a rough comparison of the sensing capability among different optical technologies and structures. Sensitivity can be enhanced by increasing the interaction between light and the biomolecules. Sensitivity is

$$S = \frac{\partial \lambda}{\partial n}. \tag{1}$$

Resolution is another important parameter to consider in characterizing a sensor's performance. Sensitivity refers to the magnitude of a sensor's response to a given change in analytes on the sensor surface, and resolution refers to the smallest change in analytes that can be measured.

Our analysis focuses on PCS structures, the periodically patterned dielectric slabs described in Fig. 1. A PCS may be entirely described by a unit cell with a lattice constant, a, an associated hole radius, r, and slab thickness, t, seen in Fig. 1a. We analyze PCS structures made of a high-index material, titanium dioxide (TiO_2, $n = 2.62$), immersed in a low-index fluid, such as water ($n = 1.33$), ethanol ($n = 1.3611$), isopropyl alcohol ($n = 1.3776$) and hydrogen peroxide ($n = 1.4061$) [30, 31]. In the symmetric case shown in Fig. 1b, the TiO_2 PCS is surrounded by liquid from above and below. In the asymmetric case shown in Fig. 1c, it is resting on a silicon dioxide (SiO_2, $n = 1.46$) substrate. Refractive index describes the optical characteristics of a medium and is defined as the ratio of the speed of light in free space over the speed of light in the medium. A substrate can compromise for example glass. Excitation is a normally incident plane wave (along the z-direction) with an electric field linearly polarized along the y-direction. The effects described here are general and apply to incident wave polarization along the x-direction as well.

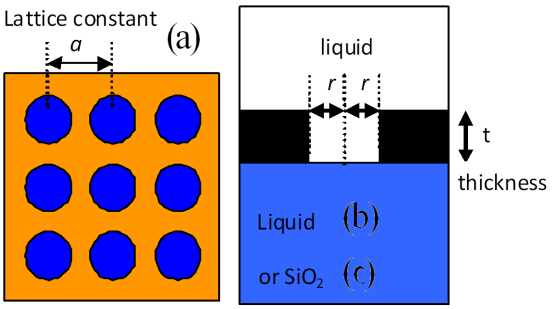

Fig. 1. (a) A unit cell for a square grid of holes PCS. Illustrations of (b) symmetric and (c) asymmetric PCS designs.

Computational technique used is MEEP [32], a freely available finite-difference time-domain (FDTD) implementation [33]. FDTD is an accurate method for determining the interaction of any physical structure with electromagnetic radiation. It involves representing the physical structure to be modeled as a 2D and 3D object consisting of materials with known dielectric permittivity. FDTD solves Maxwell's equations to determine a nearly exact representation of how the light pulse propagates through the physical structure. FDTD allows simulation of only a single "unit cell" of structure with the application of periodic boundary conditions (PBCs). PBCs are applied to the xz and yz planes to emulate infinite

planar periodicity, while perfect matched layers (PMLs) terminate the top and bottom of the unit cell to absorb outgoing fields. To solve modes of the PCS, the excitation consists of a broadband planar Gaussian source located above the PCS. Modal field distributions are calculated by exciting the PCS using a planar continuous--wave source also located above the PCS.

3. Results

Figure 1 shows symmetrical and asymmetrical structure of TiO_2 photonic crystal structure in the square lattice of holes. TiO_2 slab with high refractive indices in symmetrical structure is surrounded by fluids with refractive indices lower than TiO_2. In asymmetrical structure of the TiO_2 slab is supported by SiO_2 substrate which has lower refractive indices.

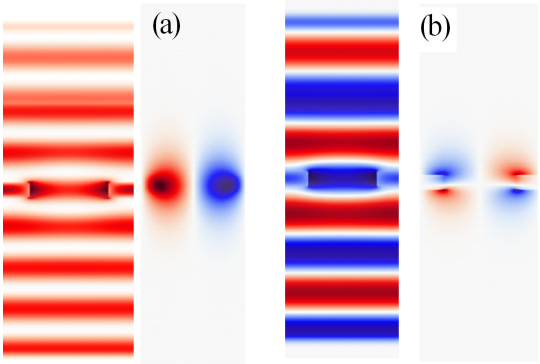

Fig. 2. TE-like guided resonance mode profile in a symmetric PCS: (a) the electric field energy density, $\varepsilon|E|2$, and (b) field profile components (E_x, E_y, E_z) for a hole radius to period ratio $r/a = 0.3$.

Figure 2 shows how a normally incident plane wave excited TE-like modes. TE-like modes have even symmetry in their electric field with respect to the mirror plane perpendicular to the vertical (z) axis [34]. As seen in Fig. 2b a PCS excited at TE-like guided resonance frequency will have its dominant electric field component coincident with that of the excitation. The periodic hole pattern (which introduces a periodic RI modulation) seen by the in-plane electric field will result in considerable scattering and a short resonating lifetime (low quality factor-Q). Hence, much of the electric field energy, $\varepsilon|E|^2$, is restricted to the dielectric and hole regions of the slab in TE-like resonance conditions.

Figure 3 shows transmission spectra for symmetric PCS designs of different slab thickness and surrounded medium excited at TE-like guided resonance frequencies. PCS incorporate these valuable properties with the ability to couple light from free-space radiation modes into guided resonances by vertical light coupling. PCS-based sensors operate by detecting minute changes in the index of refraction of a surrounding medium by observing shifts in guided resonance frequencies. The increase of

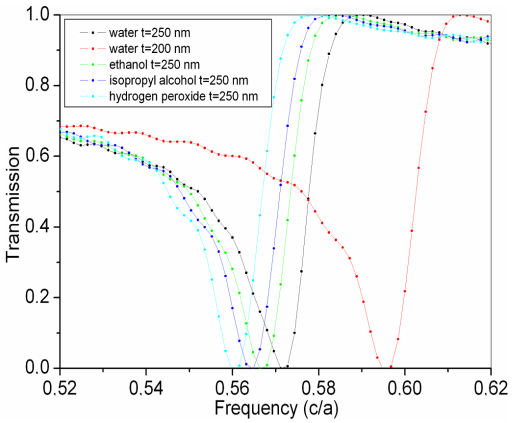

Fig. 3. TE-like mode transmission spectrum for hole radius $r = 0.3a$. Units for the electric field and electric field energy are arbitrary and consistent between plots.

refractive index of surrounded fluid causes a decrease of TE-like guided resonance frequency, as seen in Table I. Hence, scattering in PCS decreases and quality factor increases. At the same time, more interaction with electric field energy occurs in the hole region and filling factor and sensitivity values increases.

TABLE I

Symmetric photonic crystal.

Materials	Res. wav. [nm]	Sensitivity [nm/RIU]	Quality factor	Filling fraction
water	1750	333	145	0.374
hydrogen peroxide	1785	450	170	0.469
ethanol	1765	416	151	0.453
isopropyl alcohol	1770	428	155	0.459

Same situation occurs in asymmetric PCS structure. But, the value of resonance frequency shifted to lower values comparing with symmetric structure. Electric field energy density and mode profile for fundamental (lowest order) TE-like guided resonance in an asymmetric PCS design is shown in Fig. 4.

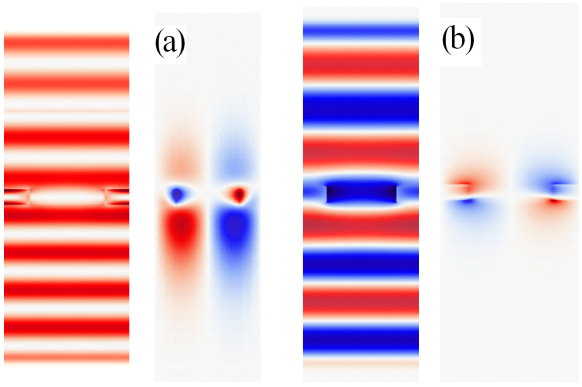

Fig. 4. TE-like guided resonance mode profile in an asymmetric PCS: (a) the electric field energy density, $\varepsilon|E|2$, and (b) field profile components (E_x, E_y, E_z) for a hole radius to period ratio $r/a = 0.3$.

Mode profiles correspond closely to those of the symmetric design. The asymmetric design does, however, introduce a RI contrast with the substrate that is smaller than that of the water superstrate. The evanescent field energy greatly affect the sensing characteristic and most of it exist in the substrate. Figure 5 shows transmission spectra for asymmetric PCS designs and surrounded medium excited at TE-like guided resonance frequencies. A summary of mode properties for the TE-like guided resonance modes from Fig. 4 is shown in Table II.

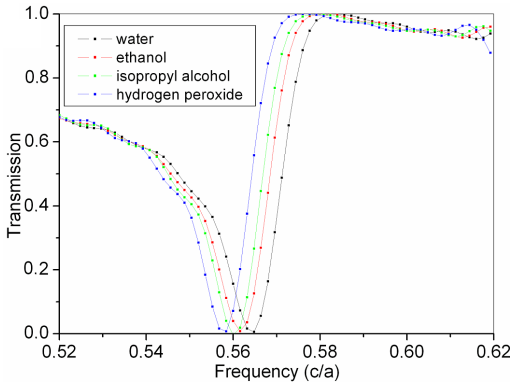

Fig. 5. TE-like mode transmission spectrum asymmetric PCS for hole radius $r = 0.3a$. Units for the electric field and electric field energy are arbitrary and consistent between plots.

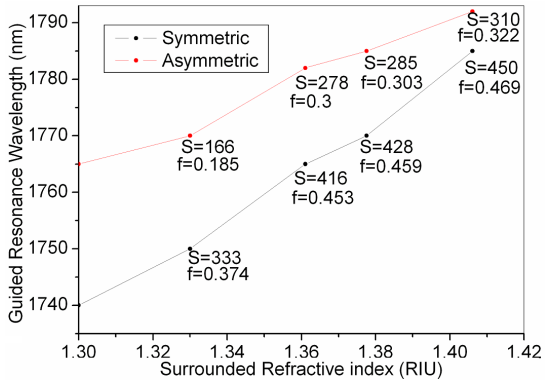

Fig. 6. Guided resonance wavelength versus surrounding RI for a symmetric PCS sensor design and an asymmetric PCS sensor design ($r = 300$ nm, $t = 250$ nm). Bulk spectral sensitivity values are indicated for surrounding RI values of between 1.30 and 1.40.

TABLE II

Asymmetric photonic crystal.

Materials	Res. wav. [nm]	Sensitivity [nm/RIU]	Quality factor	Filling fraction
water	1770	166	150	0.185
hydrogen peroxide	1792	310	180	0.322
ethanol	1782	278	165	0.300
isopropyl alcohol	1785	285	170	0.303

If we increase the refractive index of the surrounded liquid, the relative refractive index will decrease. Hence, the interaction between the applied field energy and surrounded liquid increases. Result of that the value of f and S increase, as shown in Fig. 6. However, the trend is observed that longer wavelength guided resonances will have a higher sensitivity.

As a result, to have a good correspondence between PCS biodetection analyte region and electric field energy we need to have appropriate mode selection. However, the mode profile of TE-like resonances extends less to external regions, and may be better optimized for protein and enzyme detection assays by using TiO_2 based sensors. Protein detection assays, such as for example detection protein biomarkers in bodily fluids for diagnostic tests, where proteins are present in very low concentrations.

4. Conclusions

Biosensors based on TiO_2 photonic crystal slab have high sensitivity at visible wavelengths. One of the important parameters for the optimization of the biosensors is lattice constant. In our calculation we used $a = 1000$ nm for lattice constant. The resonance wavelengths at 1500 nm are the values given in Tables I and II. This situation makes the TiO_2 material appropriate for biosensor application at visible wavelengths. Also minimum effective refractive index forms a suitable situation for the analysis of biologic tests in the sensing region and photonic crystal biosensor performance.

As a result, we investigated the TE-like modes of TiO_2 photonic crystal slab in symmetric and asymmetric structure and showed how the variation of refractive index affects the bulk spectral sensitivity and resonance quality factors. Finally, analysis of modal field distributions suggests that TE-like resonance sensors may be suited for protein and biomolecule detection.

References

[1] C. Ge, M. Lu, W. Zhang, B T. Cunningham, *Appl. Phys. Lett.* **96**, 163702 (2010).

[2] B.T. Cunningham, P. Li, S. Schulz, B. Lin, C. Baird, J. Gerstenmaier, C. Genick, F. Wang, E. Fine, L. Laing, *J. Biomol. Screen.* **9**, 481 (2004).

[3] A.J. Cunningham, *Introduction to Bioanalytical Sensors*, Wiley, NewYork 1998.

[4] N. Ganesh, I.D. Block, B.T. Cunningham, *Appl. Phys. Lett.* **89**, 23901 (2006).

[5] B. Lin, J. Qiu, J. Gerstenmeier, P. Li, H.M. Pien, J. Pepper, B. Cunningham, *Biosens. Bioelectron.* **17**, 827 (2002).

[6] L.L. Chan, S.L. Gosangari, K.L. Watkin, B.T. Cunningham, *Sens. Actuat. B* **132**, 418 (2008).

[7] C.J. Choi, A.R. Belobraydich, L.L. Chan, P.C. Mathias, B.T. Cunningham, *Anal. Biochem.* **405**, 1 (2010).

[8] M.F. Pineda, L.L.Y. Chan, T. Kuhlenschmidt, C.J. Choi, M. Kuhlenschmidt, B.T. Cunningham, *IEEE Sens. J.* **9**, 470 (2009).

[9] I.D. Block, N. Ganesh, M. Lu, B.T. Cunningham, *IEEE Sensors J.* **8**, 274 (2008).

[10] I.D. Block, L.L. Chan, B.T. Cunningham, *Sens. Actuat. B* **120**, 187 (2006).

[11] S.M. Zhang, X. Wang, *Mater. Lett.* **60**, 2143 (2006).

[12] M. Viticoli, A. Curulli, A. Cusma, S. Kaciulis, S. Nunziante, *Mater. Sci. Eng.* **26**, 947 (2006).

[13] R. Khan, M. Dhayal, *Electrochem. Commun.* **10**, 263 (2008).

[14] F. He, S. Liu, *Talanta* **62**, 271 (2004).

[15] R. Khan, M. Dhayal, *Electrochem. Commun.* **10**, 492 (2008).

[16] D. Ian, M. Pineda, J.C. Charles, B.T. Cunningham, *IEEE Sensors J.* **8**, 1546 (2008).

[17] E. Jardinier, G. Pandraud, M.H. Pham, P.J. French, P.M. Sarro, *J. Phys., Conf. Series* **187**, 012043 (2009).

[18] A.K.M. Kafi, G. Wu, A. Chen, *Biosens. Bioelectron.* **24**, 566 (2008).

[19] K.S. Mun, S.D. Alvarez, W.Y. Choi, M.J. Sailor, *ACS Nano* **4**, 2070 (2010).

[20] Y. Li, X. Liu, H. Yuan, D. Xiao, *Biosens. Bioelectron.* **24**, 706 (2009).

[21] H. Cao, Y. Zhu, L. Tang, X. Yang, C. Li, *Electroanalysis* **20**, 2223 (2008).

[22] X. Wang, M. Fujimaki, K. Awazu, *Opt. Expr.* **13**, 1486 (2005).

[23] W. Zhang, B.T. Cunningham, *Appl. Phys. Lett.* **93**, 133115 (2008).

[24] E. Graugnard, D.P. Gaillot, S.N. Dunham, C.W. Neff, T. Yamashita, C.J. Summers, *Appl. Phys. Lett.* **89**, 181108 (2006).

[25] P.C. Mathias, N. Ganesh, W. Zhang, B.T. Cunningham, *J. Appl. Phys.* **103**, 094320 (2008).

[26] J.D. Joannopulous, R.D. Meade, J.N. Winn, *Photonic Crystals: Molding the Flow of Light*, University Press, Princeton 1995.

[27] E. Yablonovitch, *Phys. Rev. Lett.* **58**, 2059 (1987).

[28] S. John, *Phys. Rev. Lett.* **58**, 2486 (1987).

[29] I.M. White, X. Fan, *Opt. Expr.* **16**, 1020 (2008).

[30] E.D. Palik, *Handbook of Optical Constants of Solids I*, Academic, New York 1985.

[31] R. Hawkings, *Handbook of Optofluidics I*, Aaron Holger Schmidt CRC, New York 2010.

[32] S.G. Johnson, J.D. Joannopoulos, *The MIT Electromagnetic Equation Propagation-Bands Package*, `http://ab-initio.mit.edu/meep/` .

[33] S.G. Johnson, J.D. Joannopoulos, *Opt. Expr.* **8**, 173 (2001).

[34] S.G. Johnson, S.H. Fan, P.R. Villeneuve, J.D. Joannopoulos, L.A. Kolodziejski, *Phys. Rev. B* **60**, 5751 (1999).